

# Vibrational properties of LaNiO<sub>3</sub> films in the ultrathin regime

**Journal Article****Author(s):**

Schober, Alexander; Fowlie, Jennifer; Guennou, Mael; Weber, Mads C.; Zhao, Hongjian; Íñiguez, Jorge; Gibert, Marta; Triscone, Jean-Marc; Kreisel, Jens

**Publication date:**

2020-06

**Permanent link:**

<https://doi.org/10.3929/ethz-b-000422257>

**Rights / license:**

[Creative Commons Attribution 4.0 International](#)

**Originally published in:**

APL Materials 8(6), <https://doi.org/10.1063/5.0010233>




**Funding acknowledgement:**

178825 - Dynamical processes in systems with strong electronic correlations (SNF)

# Vibrational properties of $\text{LaNiO}_3$ films in the ultrathin regime

Cite as: APL Mater. **8**, 061102 (2020); <https://doi.org/10.1063/5.0010233>

Submitted: 09 April 2020 . Accepted: 14 May 2020 . Published Online: 02 June 2020

Alexander Schober, Jennifer Fowlie , Mael Guennou , Mads C. Weber , Hongjian Zhao, Jorge Íñiguez, Marta Gibert, Jean-Marc Triscone, and Jens Kreisel



View Online



Export Citation



CrossMark

## ARTICLES YOU MAY BE INTERESTED IN

[Strongly correlated and topological states in \[111\] grown transition metal oxide thin films and heterostructures](#)

APL Materials **8**, 050904 (2020); <https://doi.org/10.1063/5.0009092>

[Aspects of the synthesis of thin film superconducting infinite-layer nickelates](#)

APL Materials **8**, 041107 (2020); <https://doi.org/10.1063/5.0005103>

[Emergent behavior of  \$\text{LaNiO}\_3\$  in short-periodic nickelate superlattices](#)

APL Materials **8**, 041113 (2020); <https://doi.org/10.1063/5.0004530>



AIP Conference Proceedings

**The 18th International Conference  
on Positron Annihilation**

ORDER PRINT EDITION






# Vibrational properties of $\text{LaNiO}_3$ films in the ultrathin regime

Cite as: APL Mater. 8, 061102 (2020); doi: 10.1063/5.0010233

Submitted: 9 April 2020 • Accepted: 14 May 2020 •

Published Online: 2 June 2020



Alexander Schober,<sup>1,2</sup> Jennifer Fowlie,<sup>3</sup>  Mael Guennou,<sup>1,2</sup>  Mads C. Weber,<sup>4</sup>  Hongjian Zhao,<sup>1,5</sup> Jorge Íñiguez,<sup>1,2</sup> Marta Gibert,<sup>6</sup> Jean-Marc Triscone,<sup>3</sup> and Jens Kreisel<sup>1,2</sup>

## AFFILIATIONS

<sup>1</sup>Materials Research and Technology Department, Luxembourg Institute of Science and Technology, 41 rue du Brill, L-4422 Belvaux, Luxembourg

<sup>2</sup>Department of Physics and Materials Science, University of Luxembourg, 41 rue du Brill, L-4422 Belvaux, Luxembourg

<sup>3</sup>DQMP – University of Geneva, École de Physique, 24, Quai Ernest-Ansermet, CH-1211 Geneva, Switzerland

<sup>4</sup>Department of Materials, ETH Zurich, Vladimir-Prelog-Weg 4, 8093 Zurich, Switzerland

<sup>5</sup>Physics Department and Institute for Nanoscience and Engineering University of Arkansas, Fayetteville, Arkansas 72701, USA

<sup>6</sup>Physik-Institut, University of Zurich, Winterthurerstrasse 190, 8057 Zurich, Switzerland

## ABSTRACT

Collective rotations and tilts of oxygen polyhedra play a crucial role in the physical properties of complex oxides such as magnetism and conductivity. Such rotations can be tuned by preparing thin films in which dimensionality, strain, and interface effects come into play. However, little is known of the tilt and rotational distortions in films a few unit cells thick including the question of if coherent tilt patterns survive at all in this ultrathin limit. Here, a series of films of perovskite  $\text{LaNiO}_3$  is studied and it is shown that the phonon mode related to oxygen octahedral tilts can be followed by Raman spectroscopy down to a film thickness of three pseudocubic perovskite unit cells ( $\sim 1.2$  nm). To push the limits of resolution to the ultrathin regime, a statistical analysis method is introduced to separate the Raman signals of the film and substrate. Most interestingly, these analyses reveal a pronounced hardening of the tilt vibrational mode in the thinnest films. A comparison between the experimental results, first principles simulations of the atomic structure, and the standing wave model, which accounts for size effects on the phononic properties, reveals that in the ultrathin regime, the Raman spectra are a hybrid entity of both the bulk and surface phononic behavior. These results showcase Raman spectroscopy as a powerful tool to probe the behavior of perovskite films down to the ultrathin limit.

© 2020 Author(s). All article content, except where otherwise noted, is licensed under a Creative Commons Attribution (CC BY) license (<http://creativecommons.org/licenses/by/4.0/>). <https://doi.org/10.1063/5.0010233>

## INTRODUCTION

Physical properties of complex oxides are remarkably sensitive to minute details of their crystal structure.<sup>1,2</sup> In particular, rotations or tilts of the oxygen polyhedra govern the orbital overlap between cations and oxygen-anions and can determine magnetism, electronic conductivity, metal-insulator transitions, or ferroelectricity, as a few examples.<sup>3,4</sup> In rare-earth nickelates, structural tuning by heterostructuring has been shown to cause remarkable shifts in transition temperatures through the modulation of the orbital overlaps.<sup>5,6</sup> While biaxial strain tends to extend over

tens of nanometers, octahedral tilts in perovskite oxide heterostructures can vary over single unit cell layers.<sup>7–13</sup> At an interface, particularly, strong variations can occur, opening up the possibility to design functional heterostructures. For instance, it was previously demonstrated that  $\text{LaNiO}_3$  films on the (001)<sub>pc</sub>-oriented  $\text{LaAlO}_3$  substrate display a conductivity modulated by film thickness,<sup>11</sup> eventually becoming insulating under 3 pseudocubic unit cells (pc u.c.).<sup>14–16</sup> This behavior was explained, through analyzing transmission electron microscopy images and first principles calculations, by a depth-differentiated film structure due to the heterointerface and a strong surface influence on the properties toward the atomic limit.

Even though the internal structure of these films may be strongly thickness-dependent, detailed modeling of x-ray diffraction signals has shown that the film-averaged octahedral tilts and rotations of  $\text{LaNiO}_3$  on  $\text{LaAlO}_3$  are robust and remain unchanged in magnitude down to 5 pc.u.c.<sup>17</sup>

A further experimental technique that has been successfully applied to investigate the structure of thin films and heterostructures is Raman spectroscopy.<sup>18–21</sup> Raman spectroscopy has major advantages over the techniques mentioned already: It is non-destructive and does not require large facilities. Furthermore, Raman spectroscopy allows the structural order to be traced via the so-called soft mode.<sup>22</sup> This soft-mode spectroscopy approach was previously employed in, for instance, bulk  $\text{LaAlO}_3$ <sup>23–25</sup> and  $\text{SrTiO}_3$ <sup>26</sup> to follow tilt distortions. In contrast to polar soft modes correlated with ferroelectricity,<sup>20</sup> there is, to the best of the authors' knowledge, no experimental data on how soft tilt modes behave for ultrathin films. The aim of this work is an in-depth understanding of tilt distortions in the ultrathin limit and how the corresponding Raman spectrum relates to these structural details, as the thickness is decreased from a usually well-known bulk spectrum to a two-dimensional system.

Here,  $\text{LaNiO}_3$  films of different thicknesses on the  $\text{LaAlO}_3$  substrate in  $(001)_{\text{pc}}$  pseudocubic orientation [Fig. 1(a)] are investigated by Raman spectroscopy. Both the bulk  $\text{LaNiO}_3$  and the  $\text{LaAlO}_3$  substrate are  $\text{ABO}_3$  perovskites with the same rhombohedral space group,  $R\bar{3}c$ , and tilt system, written as  $a^-a^-a^-$  in Glazer notation. Both compounds have antiphase octahedral tilts of equal magnitude ( $5.6^\circ$  in  $\text{LaAlO}_3$  and  $5.2^\circ$  in  $\text{LaNiO}_3$ <sup>27,28</sup>) about the three pseudocubic directions that can be compounded into one antiphase rotation magnitude around the  $[111]_{\text{pc}}$  vector.<sup>29</sup> Figure 1(b) displays the thick film Raman spectrum for  $\text{LaNiO}_3$  and the bulk Raman spectrum for the substrate  $\text{LaAlO}_3$ . In  $\text{LaNiO}_3$ , the octahedral rotation distortion, the order parameter of the system, is related to the only fully symmetric  $A_{1g}$  phonon mode<sup>19,30–32</sup> sketched in Fig. 1(c). The  $A_{1g}$  mode is, therefore, described as a “soft mode.” The softening of this mode with increasing temperature was evidenced in Ref. 31, in relation to a transition to the cubic phase that is not observed in practice but would occur at about 1780 K.

## EXTRACTING RAMAN SPECTRA OF ULTRATHIN FILMS

A major challenge for Raman spectroscopy on very thin films is the predominant signal of the substrate. Here, this issue is overcome by employing a specific strategy, combining confocal micro-Raman spectroscopy and principal component analysis (PCA) to extract the weak phonon signal from the films by demixing the depth-resolved spectra. The basic setup is schematized in Fig. 2(a). The signal of the film and the signal of the substrate have different depth dependencies. The film signal is the strongest for a laser focus in the vicinity of the surface, whereas the substrate signal remains strong for a laser focus deep into the sample, as sketched on the right of Fig. 2(a). These distinct evolutions with the laser focus allow the separation of film and substrate signals by multivariate analysis methods.<sup>33</sup> Here, principal component analysis (PCA) was used to treat the data. This analysis generates three important parameters—(a) The principal components: A set of individual spectra that describe the features of the measured stack of data. (b) The eigenvalues of the principal components: The larger the value, the more important the corresponding component for the dataset. (c) The score of the components: The score shows an evolution of the weight of a principal component throughout the dataset. The image in Fig. 2(b) shows an application of the method for a 7 pc.u.c. (2.7 nm)  $\text{LaNiO}_3$  sample, where the laser focal point  $z$  is varied within  $\pm 10 \mu\text{m}$  of the sample surface in  $0.2 \mu\text{m}$  steps. The eigenvalues obtained from the PCA are shown in Fig. 2(c). As can be seen, only the first two components have a significant weight and are relevant for the analysis (indicated by the blue and red squares). All other components have a very small variance and can be treated as negligible. The scores of these two components are shown in Fig. 2(d) and have a distinct behavior as a function of  $z$ , being step-like and peak-shaped, respectively. The corresponding components are displayed in Fig. 2(e) and compared with the raw spectrum. As anticipated, the first component can be associated with the substrate spectrum and shows the peaks known from  $\text{LaAlO}_3$  [see Fig. 1(b)], while the second component is associated with the film spectrum, where the characteristic peaks are clearly distinguished. Especially remarkable is the demixing of

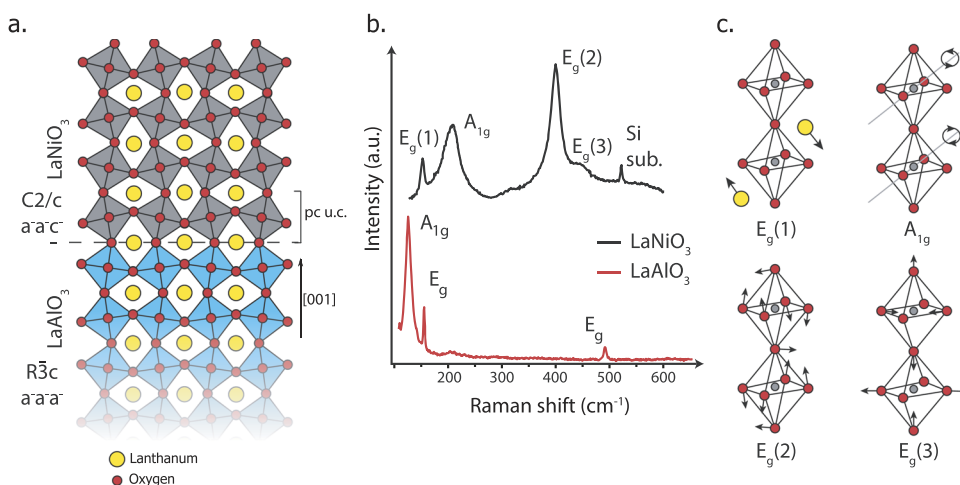


**FIG. 1.** (a) Sketch of the  $\text{LaNiO}_3$  layers on  $[001]$ -oriented  $\text{LaAlO}_3$  with the pseudocubic unit cell (pc.u.c.) indicated. (b) Raman spectra of a thick polycrystalline  $\text{LaNiO}_3$  film and a  $\text{LaAlO}_3$  substrate. (c) Atomic displacement patterns of the  $\text{LaNiO}_3$  Raman modes shown in (b), where the single  $A_{1g}$  soft mode is described as a composite octahedral rotation around the  $[111]_{\text{pc}}$  vector.

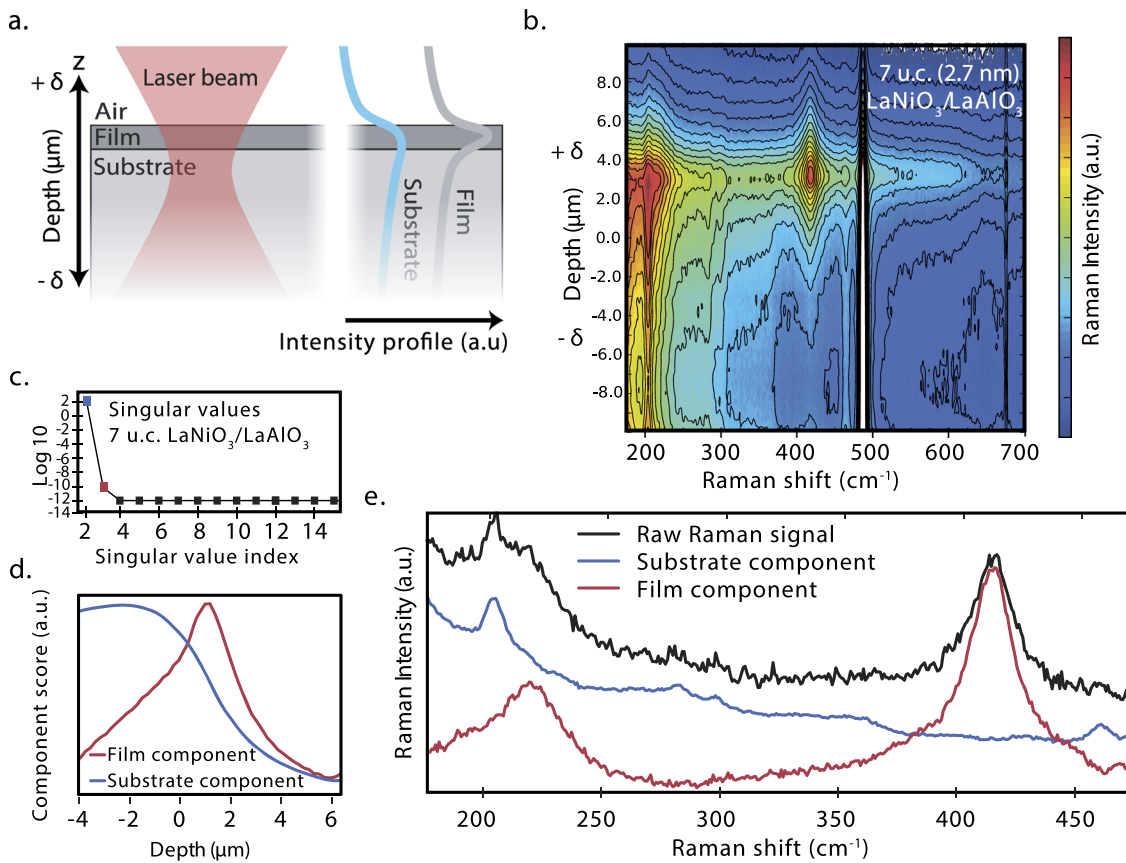


**FIG. 2.** (a) Simplified sketch of the experimental conditions and the probed volume during the micro-Raman experiment alongside the expected depth dependence of the film and substrate components (not to scale). (b) Full depth measurement dataset for 7 pc u.c. of  $\text{LaNiO}_3$  on  $\text{LaAlO}_3$ . (c) Singular value decomposition of the data shown in (b), indicating two major components indicated by the blue and red squares. (d) Principal component analysis (PCA) scores obtained on the same data for the first two components. (e) Final PCA components obtained from the depth-dependent dataset shown in (b) with the raw Raman spectrum recorded at the depth of highest film intensity (black).

the substrate and film peaks at  $210\text{--}230\text{ cm}^{-1}$ . As can be seen, this method allows the separation of the film and substrate spectra and extraction of detailed film information undisturbed by the substrate signal.

Earlier studies using depth-dependent confocal Raman spectroscopy on oxide thin films rely on the subtraction of the substrate signal.<sup>21,34</sup> Such a subtraction is based on the assumption that the spectral signature of the substrate is uniform. However, substrate responses are often modified at interfaces and between domains. Thus, a subtraction risks the introduction of artifacts. The statistical treatment of the present work compensates for varying substrate responses and allows for a clean separation of the substrate and film signal.

As displayed in Fig. 2, two Raman modes of the  $\text{LaNiO}_3$  films are accessible in this frequency range: the  $A_{1g}$  mode and one  $E_g$  mode, corresponding to tilts and bending of the  $\text{BO}_6$  octahedra [Fig. 1(c)]. The soft mode of interest is the only fully symmetric mode with  $A_{1g}$  symmetry. The mode notations relate here to the bulk rhombohedral symmetry, even though it is known that epitaxial strain stabilizes a monoclinic structure  $C2/c$  ( $a^-a^-c^-$ ), as revealed by

density functional theory (DFT) and Raman spectroscopy on films down to 14 nm.<sup>19</sup> The symmetry lowering leads to the splitting of  $E_g$  Raman peaks as well as the emergence of new peaks, but for simplicity, the labeling with respect to the bulk will be retained in this discussion.

### THICKNESS DEPENDENCE OF THE RAMAN MODES

We now apply the same measurement and analysis method to the full series of nine  $\text{LaNiO}_3$  films with thicknesses ranging from 3 pc u.c. to 15 pc u.c., as verified by x-ray diffraction and scanning transmission electron microscopy. Three representative spectra for 11 pc u.c., 7 pc u.c., and 3 pc u.c. are showcased in Fig. 3(a). Three fits associated with the film component of the data shown in Fig. 3(a) are shown in panel (b). The fits require two Lorentzian distributions for each of the Raman bands, as a consequence of the symmetry lowering from rhombohedral to monoclinic. However, only the main peak remains dominant and can be followed reliably for varying film thickness throughout the series. The weaker

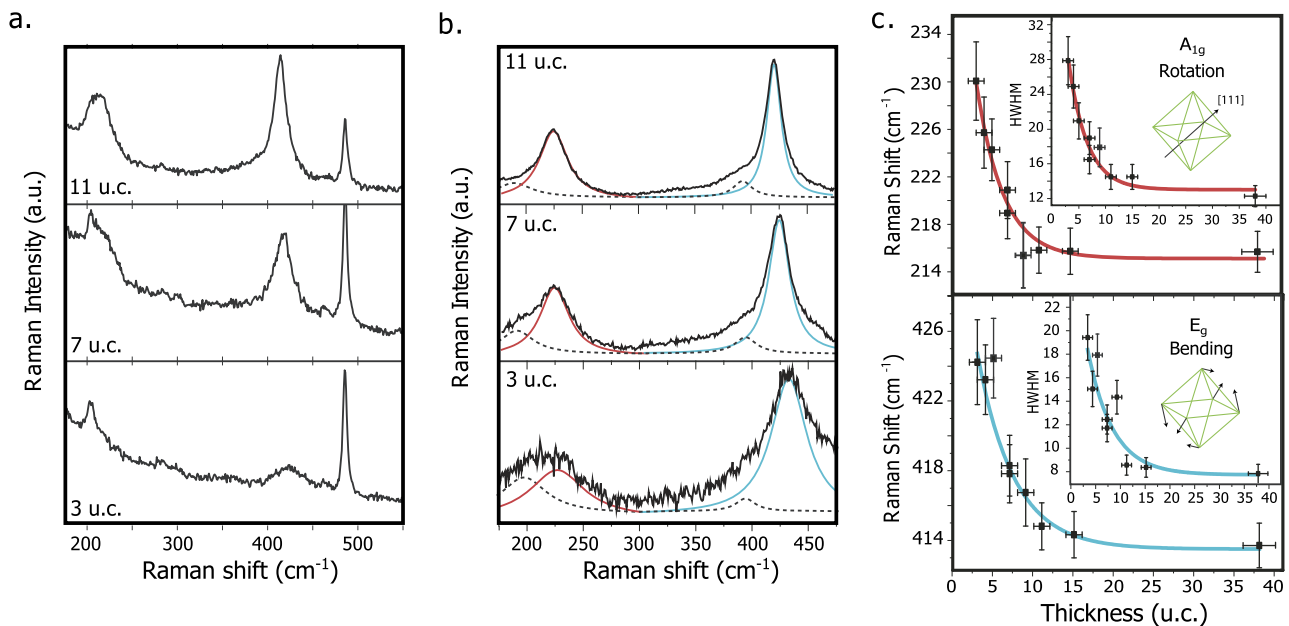


**FIG. 3.** (a) Raw Raman spectra of  $\text{LaNiO}_3$  on  $\text{LaAlO}_3$  for 3 pc u.c., 7 pc u.c., and 11 pc u.c. The spectra were chosen from the depth where the film signal is maximal. (b) Film components extracted from the PCA with the  $A_{1g}$  and  $E_g$  peaks sketched in red and blue, respectively. The additional peaks resulting from the symmetry-lowering are sketched as dashed lines. (c) Position and half width at half maximum (HWHM) of the  $\text{LaNiO}_3$   $E_g$  and  $A_{1g}$  modes resulting from the fits for the entire series of samples. Solid lines show an exponential decay fit to the data.

shoulders, shown as dotted lines in Fig. 3(b), will not be discussed further.

Figure 3(c) shows the resulting peak positions as well as the half width at half maximum (HWHM) for the  $A_{1g}$  mode (top) and  $E_g$  mode (bottom) described above for the entire series of  $\text{LaNiO}_3$  films with varying thickness. Both modes show a qualitatively similar behavior with two different regimes. For films thicker than 15 u.c., both the positions and widths are constant and coincide with the values reported in previous studies.<sup>19</sup> As thickness decreases, the mode frequency and width enter a second regime and both exhibit a pronounced increase. Figure 3(c) shows a fit of this behavior with an exponential evolution. The critical thicknesses are 8–10 u.c. (3–4 nm), and notably, the mode frequency increases for lower thicknesses, i.e., moves away from the corresponding soft mode of  $\text{LaAlO}_3$ , which is at lower frequency, as shown in Fig. 1(b), in accordance with reports on the  $E_g$  mode by Hepting and co-workers.<sup>34</sup>

### ESTIMATE OF THE RAMAN FREQUENCIES BY FIRST-PRINCIPLES

In order to provide a more thorough understanding of the Raman signature and its relation with the structure of the film, a theoretical model was constructed. Within this model, an estimate of the soft-mode frequency can be obtained directly by starting from the relaxed film structures reported previously.<sup>11</sup> These structures were obtained by running first-principles simulations in which finite  $\text{LaNiO}_3$  films of different thicknesses and the  $\text{LaAlO}_3$

substrate were treated explicitly. Then, the equilibrium solutions are distorted by moving the oxygen atoms within the  $\text{LaNiO}_3$  film so as to mimic antiphase rotations of the  $\text{O}_6$  octahedra about the  $[111]_{\text{pc}}$  axis. From this, the harmonic energy variation is computed. The energy curvature  $\kappa_{\text{soft}}$  is thus obtained, and the mode frequency can be approximated as  $\omega_{\text{soft}} = \sqrt{\kappa_{\text{soft}}/m_{\text{O}}}$ , where  $m_{\text{O}}$  is the mass of the oxygen ion. It is assumed that the eigenvector of the soft tilting mode of the  $a^-a^-c^-$ -type monoclinic films can be approximated by the well-known symmetry-determined  $A_{1g}$  eigenmode of the bulk crystal.

The results of the first-principles approach are shown in Fig. 4(a). Compared to the Raman spectra, here, a similar soft mode hardening on the order of  $20 \text{ cm}^{-1}$  is observed. The critical thickness where the mode hardening sets in is slightly reduced in the theory compared to the experiment (5 u.c. compared to 10 u.c.). These first principles calculations based on the microscopic structure, therefore, provide a reasonable description of the mode hardening in ultrathin films.

### STANDING WAVE APPROXIMATION

As an alternative, but complementary, approach, the “standing wave” approximation is considered to explain the mode hardening. This approach has proven fruitful in past studies of vibrational properties of ultrathin binary oxides films.<sup>35–40</sup> A slight adaptation is needed, however, to take into account the different symmetries of the phonon modes: these past works only report studies of polar modes, while the Raman active modes in rhombohedral  $\text{LaNiO}_3$  are



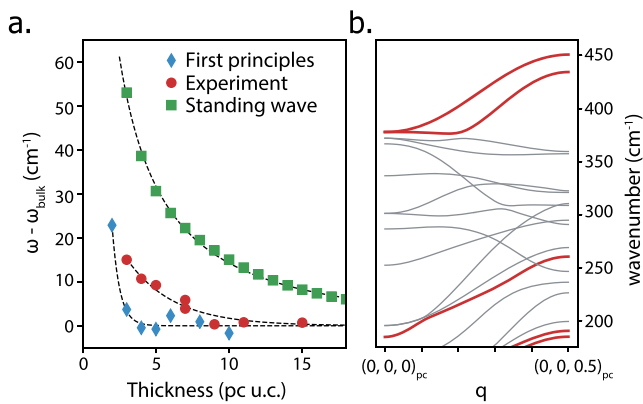


**FIG. 4.** (a) Comparison of the experimental value for the  $A_{1g}$  soft mode frequency (red circles), together with the same parameter derived from direct first principles calculation (blue diamonds) and the standing wave approach (green squares). The dashed lines are guides for the eye. (b) Phonon dispersion of bulk  $\text{LaNiO}_3$  along the  $[001]$  direction in the wavelength range of interest.

non-polar. As a result, the electrostatic boundary conditions and the dielectric properties of the media are not relevant here. Following the ideas developed in Ref. 36, we assume that non-polar modes will behave like transverse optical modes propagating perpendicular to the films, that is, without any polar component along the direction of the wavevector. The frequency of the phonon in the film is then approximated as the frequency calculated in the bulk on this phonon branch at a wavevector  $\pi/d$ , where  $d$  is the number of pseudocubic unit cells in the film. With changing film thickness, the wavevector and the frequency change according to the dispersion relation.<sup>40</sup> The boundary conditions for the approximation are represented by a wave amplitude vanishing at the interfaces. In other words, the phonon cannot propagate across the interface due to a large mismatch between the phonon frequencies of the two media.<sup>41</sup>

In practice, the phonon dispersion for bulk  $\text{LaNiO}_3$ , shown in Fig. 4(b), was calculated from first principles and the soft branch followed across the Brillouin zone. Given the complexity of the phonon dispersion relation, care was taken to follow the correct phonon branch originating from the  $A_{1g}$  tilt mode by checking the branch symmetry and the phonon eigenvector. As a result of the positive slope of the phonon branch, the soft mode frequency in the films increases as the size effect becomes more significant toward the ultrathin regime, reproducing the trend from experiment. As compared to the mode hardening seen in the Raman spectra, both the critical thickness for the hardening and the overall increase in frequency are greater. Part of this discrepancy may be due to the interface between the  $\text{LaNiO}_3$  film and the  $\text{LaAlO}_3$  substrate not establishing a sharp boundary condition—as both materials are similar in crystal structure, structural instabilities, and phonon spectrum—and, thus, reducing the effective size effect in practice.

## DISCUSSION

These Raman spectroscopy investigations into the ultrathin regime of  $\text{LaNiO}_3$  on the  $\text{LaAlO}_3$  substrate have brought to light a number of intriguing behaviors. Importantly, owing to the advanced

technical and analytical approaches employed here, both the soft phonon mode associated with the tilts and the octahedral bending mode remained measurable by Raman spectroscopy down to 3 pc u.c. (1.2 nm)—a thickness around which the distorted unit cell itself is almost undefined. Both the  $A_{1g}$  and the  $E_g$  modes show a very similar hardening beginning below 10 pc u.c.

This picture differs from a number of conventional interpretations of Raman spectra of thin films. In particular, the possibility that the shifts of Raman modes are due to a relaxation of epitaxial strain was put forward in a previous study on the  $E_g$  bending mode of  $\text{LaNiO}_3$  films<sup>34</sup> but can be ruled out here as all the films studied were epitaxially strained to the substrate. Moreover, as the global  $\text{LaNiO}_3$  octahedral rotations and tilts were found, by x-ray diffraction, not to vary with thickness down to 5 pc u.c.,<sup>17</sup> it appears that, in contrast with bulk systems, the  $A_{1g}$  mode frequency no longer scales linearly with the tilt angle. However, the bulk linear scaling follows a slope on the order of  $20\text{--}30\text{ cm}^{-1}/^\circ$  in the similarly structured chromates and ferrites.<sup>42,43</sup> This suggests that the tilt could increase by as little as one degree toward the ultrathin limit, which would be within the experimental error of the x-ray diffraction signal fitting reported previously.

On the other hand, it is remarkable that the two observed modes—both bending and tilting—of  $\text{LaNiO}_3$  exhibit very similar hardenings, with the same critical thickness, and shifts of nearly equal amplitudes. The standing wave approach employed here partially explains this behavior as both modes have an increase in frequency when moving away from the zone center. Therefore, the observation that both our Raman modes undergo a similar hardening is likely to be material-dependent. Recent reports on ultrathin  $\text{BaTiO}_3$  films<sup>40</sup> show a contrasting behavior for different modes. This underlines that the vibrational frequencies in the ultrathin limit indeed depend on the mode details and dispersion. The frequency increase in  $\text{LaNiO}_3$  that is predicted by the standing wave approach is, however, greater in magnitude than that observed in practice, but as discussed, this could stem from vibrational continuity into the substrate.

A comparison with the first-principles results shows that a purely microscopic simulation of the soft mode frequency can go a reasonable way to reproducing the same hardening behavior. As found previously by first-principles calculations and corroborated by experiment,<sup>11</sup> the  $\text{LaNiO}_3$  surface tends to dominate the overall properties toward the ultrathin limit. Ultimately, for the thinnest films, the energy variation—and, therefore, the Raman frequency—is determined by a region of the film that is relatively stiff against the  $\text{NiO}_6$  tilting mode. The complete thickness-dependence is not fully described in this picture, however, with the onset of the mode hardening taking place at 10 pc u.c. in the experiment.

The experimental mode hardening follows a trend that is part way between that predicted by the direct first-principles estimate and that predicted by the standing wave approximation. This leads toward the natural conclusion that, in this ultrathin regime, the thin film cannot be considered as simply a slice of the bulk crystal but rather as a hybrid entity. Therefore, discussion of both the phononic behavior of a crystalline solid and the vibrational properties of a surface is required.

These results showcase Raman spectroscopy coupled with principal component analysis as an efficient tool to investigate vibrational properties in severely reduced sample dimensions. This

method is entirely general and can potentially be implemented in more complex systems—in terms of symmetry and number of modes—than  $\text{LaNiO}_3$  on the  $\text{LaAlO}_3$  substrate. Interestingly, the change in metallicity due to the altered film thicknesses<sup>11</sup> does not impact the quality of the PCA. This further underlines the universality of our approach. Modes corresponding to the oxygen octahedral tilting and bending could still be identified in films as thin as 3 pseudocubic unit cells or 1.2 nm—a testament both to the power of the analysis technique and to the high quality of the thin films. Both of these modes are found to harden significantly toward the atomic limit. The onset of the hardening cannot be fully accounted for by microscopic considerations alone. Incorporating a standing wave approach, commonly employed in the study of surface vibrations, sheds light on the possibility of an unexpected phononic behavior in this pseudo-2D regime that should be general to ultrathin films as a whole.

## METHODS

### Sample preparation

The samples were grown by radio frequency off-axis magnetron sputtering at a temperature of 510 °C and a pressure of 0.18 mTorr ( $\text{Ar}:\text{O}_2$  7:2 mix). The series ranges from 3 to 15 unit cells. The films were characterized by x-ray diffraction, atomic force microscopy, and scanning transmission electron microscopy and were found to be coherently strained, with an atomically flat surface and high crystalline quality.<sup>11</sup>

### Raman spectroscopy

The experiments were performed, at room temperature, with a Renishaw inVia micro-Raman spectrometer. The excitation wavelength was 633 nm, with laser power lower than 1 mW. The exciting light is focused via a  $\times 100$  microscope objective with numerical aperture 0.9, resulting in nominal spot size and depths of the field of 0.86  $\mu\text{m}$  and 1.38  $\mu\text{m}$ , respectively. The scattered light was analyzed with a holographic grating with 2400 g/mm and collected on a CCD detector. All data treatments (principal component analysis and fitting with standard Lorentzian line shapes) were performed with a python-based software developed in house.

### Ab initio calculation details

We used density functional theory (DFT) as within the local density approximation (LDA), as implemented in the Vienna *ab initio* simulation package (VASP).<sup>44,45</sup> We treated the ionic cores within the so-called projector-augmented wave (PAW) approach,<sup>46</sup> solving explicitly for the following electrons: La 5*p*, 5*d*, and 6*s*; Ni 3*p*, 3*d*, and 4*s*; Al 3*s* and 3*p*; and O 2*s* and 2*p*. The 3*d* electrons of Ni were treated at the bare LDA level, which has been shown to be the most realistic way to treat metallic  $\text{LaNiO}_3$ .<sup>47</sup> Details about the structures combining the  $\text{LaNiO}_3$  film and  $\text{LaAlO}_3$  substrate are described in some detail in Ref. 11. For our phonon calculations for bulk  $\text{LaNiO}_3$ , we used the usual 10-atom primitive cell of this compound. Electronic wave functions were represented in a plane-wave basis truncated at 400 eV and 500 eV, respectively, for our  $\text{LaNiO}_3/\text{LaAlO}_3(001)$  and bulk  $\text{LaNiO}_3$  simulations. Reciprocal space integrals were computed using a  $5 \times 5 \times 1$  *k*-point mesh in

our  $\text{LaNiO}_3/\text{LaAlO}_3(001)$  calculations, while a mesh of  $8 \times 8 \times 8$  *k*-points was used to treat bulk  $\text{LaNiO}_3$  in its 10-atom primitive cell. We used phonopy<sup>48</sup> for the calculation of phonon bands, using a  $2 \times 2 \times 2$  multiple of the 10-atom primitive cell (and, correspondingly, a  $4 \times 4 \times 4$  *k*-point grid).

## AUTHORS' CONTRIBUTIONS

J.F. fabricated and characterized the samples. A.S. performed the Raman experiments and developed the tools for their analysis with input from M. Guennou. M.C.W. initiated the use of a multivariate analysis method to study ultrathin films. H.Z. and J.I. performed and analyzed the DFT calculations. J.-M.T. and J.K. directed the research. All authors contributed to the analysis of the results and the preparation of this manuscript.

## ACKNOWLEDGMENTS

A.S., M. Guennou, H.Z., J.I., and J.K. acknowledge support from the Luxembourg National Research Fund under Project No. CO-FERMAT FNR/P12/4853155/Kreisel and the AFR, Grant No. 7749159. M.C.W. acknowledges support from SNSF (Grant No. 200021\_178825). M. Gibert acknowledges financial support through the SNSF, Grant No. PP00P2\_170564. This work was supported by the Swiss National Science Foundation through Division II. The research leading to these results has received funding from the European Research Council under the European Union's Seventh Framework Program (No. FP7/2007-2013)/ERC Grant Agreement No. 319286 (Q-MAC). M. Guennou also gratefully acknowledges discussion and input from W. Widdra (MPI of Microstructure Physics, Halle, Germany).

## DATA AVAILABILITY

The data that support the findings of this study are available from the corresponding author upon reasonable request.

## REFERENCES

- R. H. Mitchell, *Perovskites: Modern and Ancient* (Almaz Press, Ontario, Canada, 2002).
- J. B. Goodenough, "Electronic and ionic transport properties and other physical aspects of perovskites," *Rep. Prog. Phys.* **67**, 1915 (2004).
- J. M. Rondinelli, S. J. May, and J. W. Freeland, "Control of octahedral connectivity in perovskite oxide heterostructures: An emerging route to multifunctional materials discovery," *MRS Bull.* **37**, 261–270 (2012).
- J. Nordlander, M. Campanini, M. D. Rossell, R. Erni, Q. N. Meier, A. Cano, N. A. Spaldin, M. Fiebig, and M. Trassin, "The ultrathin limit of improper ferroelectricity," *Nat. Commun.* **10**, 5591 (2019).
- S. Catalano, M. Gibert, J. Fowlie, J. Iniguez, J.-M. Triscone, and J. Kreisel, "Rare-earth nickelates  $\text{RNiO}_3$ : Thin films and heterostructures," *Rep. Prog. Phys.* **81**, 046501 (2018).
- S. Middey, J. Chakhalian, P. Mahadevan, J. W. Freeland, A. J. Millis, and D. D. Sarma, "Physics of ultrathin films and heterostructures of rare-earth nickelates," *Annu. Rev. Mater. Res.* **46**, 305–334 (2016).
- R. Aso, D. Kan, Y. Shimakawa, and H. Kurata, "Atomic level observation of octahedral distortions at the perovskite oxide heterointerface," *Sci. Rep.* **3**, 2214 (2013).



- <sup>8</sup>W. Lu, W. Song, P. Yang, J. Ding, G. M. Chow, and J. Chen, "Strain engineering of octahedral rotations and physical properties of SrRuO<sub>3</sub> films," *Sci. Rep.* **5**, 10245 (2015).
- <sup>9</sup>Z. Liao, M. Huijben, Z. Zhong, N. Gauquelin, S. Macke, R. J. Green, S. Van Aert, J. Verbeeck, G. Van Tendeloo, K. Held, G. A. Sawatzky, G. Koster, and G. Rijnders, "Controlled lateral anisotropy in correlated manganite heterostructures by interface-engineered oxygen octahedral coupling," *Nat. Mater.* **15**, 425 (2016).
- <sup>10</sup>D. Kan, R. Aso, R. Sato, M. Haruta, H. Kurata, and Y. Shimakawa, "Tuning magnetic anisotropy by interfacially engineering the oxygen coordination environment in a transition metal oxide," *Nat. Mater.* **15**, 432 (2016).
- <sup>11</sup>J. Fowlie, M. Gibert, G. Tieri, A. Gloter, J. Íñiguez, A. Filippetti, S. Catalano, S. Gariglio, A. Schöber, M. Guennou, J. Kreisel, O. Stéphan, and J.-M. Triscone, "Conductivity and local structure of LaNiO<sub>3</sub> thin films," *Adv. Mater.* **29**, 1605197 (2017).
- <sup>12</sup>A. Y. Borisevich, H. J. Chang, M. Huijben, M. P. Oxley, S. Okamoto, M. K. Niranjan, J. D. Burton, E. Y. Tsybal, Y. H. Chu, P. Yu, R. Ramesh, S. V. Kalinin, and S. J. Pennycook, "Suppression of octahedral tilts and associated changes in electronic properties at epitaxial oxide heterostructure interfaces," *Phys. Rev. Lett.* **105**, 087204 (2010).
- <sup>13</sup>A. Vaillonis, H. Boschker, Z. Liao, J. R. A. Smit, G. Rijnders, M. Huijben, and G. Koster, "Symmetry and lattice mismatch induced strain accommodation near and away from correlated perovskite interfaces," *Appl. Phys. Lett.* **105**, 131906 (2014).
- <sup>14</sup>R. Scherwitzl, S. Gariglio, M. Gabay, P. Zubko, M. Gibert, and J.-M. Triscone, "Metal-insulator transition in ultrathin LaNiO<sub>3</sub> films," *Phys. Rev. Lett.* **106**, 246403 (2011).
- <sup>15</sup>J. Son, P. Moetafak, J. M. LeBeau, D. Ouellette, L. Balents, S. J. Allen, and S. Stemmer, "Low-dimensional Mott material: Transport in ultrathin epitaxial LaNiO<sub>3</sub> films," *Appl. Phys. Lett.* **96**, 062114 (2010).
- <sup>16</sup>D. P. Kumah, A. S. Disa, J. H. Ngai, H. Chen, A. Malashevich, J. W. Reiner, S. Ismail-Beigi, F. J. Walker, and C. H. Ahn, "Tuning the structure of nickelates to achieve two-dimensional electron conduction," *Adv. Mater.* **26**, 1935–1940 (2014).
- <sup>17</sup>J. Fowlie, C. Lichtensteiger, M. Gibert, H. Meley, P. Willmott, and J.-M. Triscone, "Thickness-dependent perovskite octahedral distortions at heterointerfaces," *Nano Lett.* **19**, 4188–4194 (2019).
- <sup>18</sup>J. Kreisel, M. C. Weber, N. Dix, F. Sánchez, P. A. Thomas, and J. Fontcuberta, "Probing individual layers in functional oxide multilayers by wavelength-dependent Raman scattering," *Adv. Funct. Mater.* **22**, 5044–5049 (2012).
- <sup>19</sup>M. C. Weber, M. Guennou, N. Dix, D. Pesquera, F. Sánchez, G. Herranz, J. Fontcuberta, L. López-Conesa, S. Estradé, F. Peiró, J. Íñiguez, and J. Kreisel, "Multiple strain-induced phase transitions in LaNiO<sub>3</sub> thin films," *Phys. Rev. B* **94**, 014118 (2016).
- <sup>20</sup>D. A. Tenne, A. Bruchhausen, N. D. Lanzillotti-Kimura, A. Fainstein, R. S. Katiyar, A. Cantarero, A. Soukiasian, V. Vaithyanathan, J. H. Haeni, W. Tian, D. G. Schlom, K. J. Choi, D. M. Kim, C. B. Eom, H. P. Sun, X. Q. Pan, Y. L. Li, L. Q. Chen, Q. X. Jia, S. M. Nakhmanson, K. M. Rabe, and X. X. Xi, "Probing nanoscale ferroelectricity by ultraviolet Raman spectroscopy," *Science* **313**, 1614 (2006).
- <sup>21</sup>M. Hepting, M. Minola, G. Cristiani, G. Logvenov, E. Schierle, M. Wu, M. Bluschke, E. Weschke, H.-U. Habermeier, E. Benckiser, M. Le Tacon, and B. Keimer, "Tunable charge and spin order in PrNiO<sub>3</sub> thin films and superlattices," *Phys. Rev. Lett.* **113**, 227206 (2014).
- <sup>22</sup>J. F. Scott, "Soft-mode spectroscopy: Experimental studies of structural phase transitions," *Rev. Mod. Phys.* **46**, 83 (1974).
- <sup>23</sup>J. F. Scott, "Raman study of trigonal-cubic phase transitions in rare-earth aluminates," *Phys. Rev.* **183**, 823 (1969).
- <sup>24</sup>S. A. Hayward, F. D. Morrison, S. A. T. Redfern, E. K. H. Salje, J. F. Scott, K. S. Knight, S. Tarantino, A. M. Glazer, V. Shuvaeva, P. Daniel, M. Zhang, and M. A. Carpenter, "Transformation processes in LaAlO<sub>3</sub>: Neutron diffraction, dielectric, thermal, optical, and Raman studies," *Phys. Rev. B* **72**, 054110 (2005).
- <sup>25</sup>P. Bouvier and J. Kreisel, "Pressure-induced phase transition in LaAlO<sub>3</sub>," *J. Phys.: Condens. Matter* **14**, 3981 (2002).
- <sup>26</sup>P. A. Fleury, J. F. Scott, and J. M. Worlock, "Soft phonon modes and the 110 K phase transition in SrTiO<sub>3</sub>," *Phys. Rev. Lett.* **21**, 16–19 (1968).
- <sup>27</sup>K. A. Müller, W. Berlinger, and F. Waldner, "Characteristic structural phase transition in perovskite-type compounds," *Phys. Rev. Lett.* **21**, 814 (1968).
- <sup>28</sup>J. L. García-Muñoz, J. Rodríguez-Carvajal, P. Lacorre, and J. B. Torrance, "Neutron-diffraction study of RNiO<sub>3</sub> (R = La, Pr, Nd, Sm): Electronically induced structural changes across the metal-insulator transition," *Phys. Rev. B* **46**, 4414 (1992).
- <sup>29</sup>A. M. Glazer, "Simple ways of determining perovskite structures," *Acta Crystallogr., Sect. A* **31**, 756 (1975).
- <sup>30</sup>M. V. Abrashev, A. P. Litvinchuk, M. N. Iliev, R. L. Meng, V. N. Popov, V. G. Ivanov, R. A. Chakalov, and C. Thomsen, "Comparative study of optical phonons in the rhombohedrally distorted perovskites LaAlO<sub>3</sub> and LaMnO<sub>3</sub>," *Phys. Rev. B* **59**, 4146–4153 (1999).
- <sup>31</sup>N. Chaban, M. Weber, S. Pignard, and J. Kreisel, "Phonon Raman scattering of perovskite LaNiO<sub>3</sub> thin films," *Appl. Phys. Lett.* **97**, 031915 (2010).
- <sup>32</sup>G. Gou, I. Grinberg, A. M. Rappe, and J. M. Rondinelli, "Lattice normal modes and electronic properties of the correlated metal LaNiO<sub>3</sub>," *Phys. Rev. B* **84**, 144101 (2011).
- <sup>33</sup>J. Kunc, Y. Hu, J. Palmer, C. Berger, and W. A. de Heer, "A method to extract pure Raman spectrum of epitaxial graphene on SiC," *Appl. Phys. Lett.* **103**, 201911 (2013).
- <sup>34</sup>M. Hepting, D. Kukuruznyak, E. Benckiser, M. Le Tacon, and B. Keimer, "Raman light scattering on ultra-thin films of LaNiO<sub>3</sub> under compressive strain," *Physica B* **460**, 196–198 (2015).
- <sup>35</sup>G. Benedek and J. P. Toennies, "Helium atom scattering spectroscopy of surface phonons: Genesis and achievements," *Surf. Sci.* **299–300**, 587–611 (1994).
- <sup>36</sup>P. Senet, P. Lambin, and A. A. Lucas, "Standing-wave optical phonons confined in ultrathin overlayers of ionic materials," *Phys. Rev. Lett.* **74**, 570–573 (1995).
- <sup>37</sup>L. Savio, E. Celasco, L. Vattuone, M. Rocca, and P. Senet, "MgO/Ag(100): Confined vibrational modes in the limit of ultrathin films," *Phys. Rev. B* **67**, 075420 (2003).
- <sup>38</sup>V. Goian, F. O. Schumann, and W. Widdra, "Growth and lattice dynamics of ultrathin BaO films on Pt(001)," *J. Phys.: Condens. Matter* **30**, 095001 (2018).
- <sup>39</sup>L. Vattuone, L. Savio, and M. Rocca, "Phonons in thin oxide films," in *Oxide Materials at the Two-Dimensional Limit* (Springer, 2016), pp. 169–199.
- <sup>40</sup>J. Premper, F. O. Schumann, A. Dhaka, S. Polzin, K. L. Kostov, V. Goian, D. Sander, and W. Widdra, "Surface stress and lattice dynamics in oxide ultrathin films," *Phys. Status Solidi B* (published online 2020).
- <sup>41</sup>B. K. Ridley, *Electrons and Phonons in Semiconductor Multilayers* (Cambridge University Press, 2009).
- <sup>42</sup>M. C. Weber, J. Kreisel, P. A. Thomas, M. Newton, K. Sardar, and R. I. Walton, "Phonon Raman scattering of RCrO<sub>3</sub> perovskites (R = Y, La, Pr, Sm, Gd, Dy, Ho, Yb, Lu)," *Phys. Rev. B* **85**, 054303 (2012).
- <sup>43</sup>M. C. Weber, M. Guennou, H.-J. Zhao, J. Íñiguez, R. Vilarinho, A. Almeida, J. A. Moreira, and J. Kreisel, "Raman spectroscopy of rare-earth orthoferrites RFeO<sub>3</sub> (R = La, Sm, Eu, Gd, Tb, Dy)," *Phys. Rev. B* **94**, 214103 (2016).
- <sup>44</sup>G. Kresse and J. Furthmüller, "Efficient iterative schemes for *ab initio* total-energy calculations using a plane-wave basis set," *Phys. Rev. B* **54**, 11169–11186 (1996).
- <sup>45</sup>G. Kresse and D. Joubert, "From ultrasoft pseudopotentials to the projector augmented-wave method," *Phys. Rev. B* **59**, 1758–1775 (1999).
- <sup>46</sup>P. E. Blöchl, "Projector augmented-wave method," *Phys. Rev. B* **50**, 17953–17979 (1994).
- <sup>47</sup>M. Gibert, P. Zubko, R. Scherwitzl, J. Íñiguez, and J.-M. Triscone, "Exchange bias in LaNiO<sub>3</sub>–LaMnO<sub>3</sub> superlattices," *Nat. Mater.* **11**, 195–198 (2012).
- <sup>48</sup>A. Togo and I. Tanaka, "First principles phonon calculations in materials science," *Scr. Mater.* **108**, 1–5 (2015).